

Globally strictly convex cost functional for a 1-D inverse medium scattering problem with experimental data*

Michael V. Klibanov ^{†‡}; Aleksandr E. Kolesov ^{‡§};
Lam Nguyen,[¶] and Anders Sullivan[¶]

October 28, 2018

Abstract

A new numerical method is proposed for a 1-D inverse medium scattering problem with multi-frequency data. This method is based on the construction of a weighted cost functional. The weight is a Carleman Weight Function (CWF). In other words, this is the function, which is present in the Carleman estimate for the underlying differential operator. The presence of the CWF makes this functional strictly convex on any a priori chosen ball with the center at $\{0\}$ in an appropriate Hilbert space. Convergence of the gradient minimization method to the exact solution starting from any point of that ball is proven. Computational results for both computationally simulated and experimental data show a good accuracy of this method.

Key Words: global convergence, coefficient inverse problem, multi-frequency data, Carleman weight function

2010 Mathematics Subject Classification: 35R30.

1 Introduction

The experimental data used in this paper were collected by the Forward Looking Radar of the US Army Research Laboratory [40]. That radar was built for detection and possible identification of shallow explosive-like targets. Since targets are three dimensional objects, one needs to measure a three dimensional information about each target. However, the radar measures only one time dependent curve for each target, see Figure 5. Therefore, one can hope to reconstruct only a very limited information about each target. So, we

*The work of MVK and AEK was supported by US Army Research Laboratory and US Army Research Office grant W911NF-15-1-0233 and by the Office of Naval Research grant N00014-15-1-2330.

[†]The corresponding author

[‡]Department of Mathematics & Statistics, University of North Carolina at Charlotte, Charlotte, NC 28223, USA

[§]Institute of Mathematics and Information Science, North-Eastern Federal University, Yakutsk, Russia

[¶]US Army Research Laboratory, 2800 Powder Mill Road Adelphi, MD 20783-1197, USA

reconstruct only an estimate of the dielectric constant of each target. For each target, our estimate likely provides a sort of an average of values of its spatially distributed dielectric constant. But even this information can be potentially very useful for engineers. Indeed, currently the radar community is relying only on the energy information of radar images, see, e.g. [47]. Estimates of dielectric constants of targets, if taken alone, cannot improve the current false alarm rate. However, these estimates can be potentially used as an additional piece of information. Being combined with the currently used energy information, this piece of the information might result in the future in new classification algorithms, which might improve the current false alarm rate.

An Inverse Medium Scattering Problem (IMSP) is often also called a Coefficient Inverse Problem (CIP). IMSPs/CIPs are both ill-posed and highly nonlinear. Therefore, an important question to address in a numerical treatment of such a problem is: *How to reach a sufficiently small neighborhood of the exact coefficient without any advanced knowledge of this neighborhood?* The size of this neighborhood should depend only on the level of noise in the data and on approximation errors. We call a numerical method, which has a rigorous guarantee of achieving this goal, *globally convergent method* (GCM).

In this paper we develop analytically a new globally convergent method for a 1-D Inverse Medium Scattering Problem (IMSP) with the data generated by multiple frequencies. In addition to the analytical study, we test this method numerically using both computationally simulated and the above mentioned experimental data.

First, we derive a nonlinear integro-differential equation in which the unknown coefficient is not present. The *new element* of this paper is the method of the solution of this equation. This method is based on the construction of a weighted least squares cost functional. The key point of this functional is the presence of the Carleman Weight Function (CWF) in it. This is the function, which is involved in the Carleman estimate for the underlying differential operator. We prove that, given a closed ball of an arbitrary radius $R > 0$ with the center at $\{0\}$ in an appropriate Hilbert space, one can choose the parameter $\lambda > 0$ of the CWF in such a way that this functional becomes strictly convex on that ball.

The existence of the unique minimizer on that closed ball as well as convergence of minimizers to the exact solution when the level of noise in the data tends to zero are proven. In addition, it is proven that the gradient projection method reaches a sufficiently small neighborhood of the exact coefficient if its starting point is an arbitrary point of that ball. The size of that neighborhood is proportional to the level of noise in the data. Therefore, since restrictions on R are not imposed in our method, then this is a *globally convergent* numerical method. We note that in the conventional case of a non convex cost functional a gradient-like method converges to the exact solution only if its starting point is located in a sufficiently small neighborhood of this solution: this is due to the phenomenon of multiple local minima and ravines of such functionals.

Unlike previously developed globally convergent numerical methods of the first type for CIPs (see this section below), the convergence analysis for the technique of the current paper does not impose a smallness condition on the interval (\underline{k}, \bar{k}) of the variations of the wave numbers $k \in (\underline{k}, \bar{k}) \subset \{k > 0\}$.

The majority of currently known numerical methods of solutions of nonlinear ill-posed problems use the nonlinear optimization. In other words, a least squares cost functional is minimized in each problem, see, e.g. [14, 17, 18, 19]. However, the major problem with these functionals is that they are usually non convex. Figure 1 of the paper [44] presents

a numerical example of multiple local minima and ravines of non-convex least squares cost functionals for some CIPs. Hence, convergence of the optimization process of such a functional to the exact solution can be guaranteed only if a good approximation for that solution is known in advance. However, such an approximation is rarely available in applications. This prompts the development of globally convergent numerical methods for CIPs, see, e.g. [8, 9, 10, 15, 23, 24, 25, 26, 29, 31, 32, 33, 34, 35, 39, 48].

The first author with coauthors has proposed two types of GCM for CIPs with single measurement data. The GCM of the first type is reasonable to call the “tail functions method”. This development has started from the work [8] and has been continued since then, see, e.g. [9, 15, 31, 32, 34, 35, 39, 48] and references cited therein. In this case, on each step of an iterative process one solves the Dirichlet boundary value problem for a certain linear elliptic PDE, which depends on that iterative step. The solution of this PDE allows one to update the unknown coefficient first and then to update a certain function, which is called “the tail function”. The convergence theorems for this method impose a smallness condition on the interval of the variation of either the parameter $s > 0$ of the Laplace transform of the solution of a hyperbolic equation or of the wave number $k > 0$ in the Helmholtz equation. Recall that the method of this paper does not impose the latter assumption.

In this paper we present a new version of the GCM of the second type. In any version of the GCM of the second type a weighted cost functional with a CWF in it is constructed. The same properties of the global strict convexity and the global convergence of the gradient projection method hold as the ones indicated above. The GCM of the second type was initiated in [24, 25, 26] with a recently renewed interest in [10, 29, 33]. The idea of any version of the GCM of the second type has direct roots in the method of [11], which is based on Carleman estimates and which was originally designed in [11] only for proofs of uniqueness theorems for CIPs, also see the recent survey in [27].

Another version of the GCM with a CWF in it was recently developed in [6] for a CIP for the hyperbolic equation $w_{tt} = \Delta w + a(x)w + f(x, t)$, where $a(x)$ is the unknown coefficient. This GCM was tested numerically in [7]. In [6, 7] non-vanishing conditions are imposed: it is assumed that either $f(x, 0) \neq 0$ or $w(x, 0) \neq 0$ or $w_t(x, 0) \neq 0$ in the entire domain of interest. Similar assumptions are imposed in [10, 29] for the GCM of the second type. On the other hand, we consider in the current paper, so as in [24, 25, 26, 33], the fundamental solution of the corresponding PDE. The differences between the fundamental solutions of those PDEs and solutions satisfying non-vanishing conditions cause quite significant differences between [24, 25, 26, 33] and [6, 7, 10, 29] of corresponding versions of the GCM of the second type.

Recently, the idea of the GCM of the second type was extended to the case of ill-posed Cauchy problems for quasilinear PDEs, see the theory in [28] and some extensions and numerical examples in [4, 30].

CIPs of wave propagation are a part of a bigger subfield, Inverse Scattering Problems (ISPs). ISPs attract a significant attention of the scientific community. In this regard we refer to some direct methods which successfully reconstruct positions, sizes and shapes of scatterers without iterations [12, 13, 20, 22, 36, 37, 38, 45]. We also refer to [3, 37, 41, 42] for some other ISPs in the frequency domain. In addition, we cite some other numerical methods for ISPs considered in [2, 5, 46].

As to the CIPs with multiple measurement, i.e. the Dirichlet-to-Neumann map data, we mention recent works [1, 21, 43] and references cited therein, where reconstruction

procedures are developed, which do not require a priori knowledge of a small neighborhood of the exact coefficient.

In section 2 we state our inverse problem. In section 3 we construct that weighted cost functional. In section 4 we prove the main property of this functional: its global strict convexity. In section 5 we prove the global convergence of the gradient projection method of the minimization of this functional. Although this paper is mostly an analytical one (sections 3-5), we complement the theory with computations. In section 6 we test our method on computationally simulated data. In section 7 we test it on experimental data. Concluding remarks are in section 8.

2 Problem statement

2.1 Statement of the inverse problem

Let the function $c(x)$, $x \in \mathbb{R}$ be the spatially distributed dielectric constant of the medium. We assume that

$$c \in C^2(\mathbb{R}), c(x) \geq 1, \forall x \in \mathbb{R}, \quad (2.1)$$

$$c(x) = 1, \forall x \notin (0, 1). \quad (2.2)$$

Fix the source position $x_0 < 0$. For brevity, we do not indicate below dependence of our functions on x_0 . Consider the 1-D Helmholtz equation for the function $u(x, k)$,

$$u'' + k^2 c(x) u = -\delta(x - x_0), x \in \mathbb{R}, \quad (2.3)$$

$$\lim_{x \rightarrow \infty} (u' + iku) = 0, \lim_{x \rightarrow -\infty} (u' - iku) = 0. \quad (2.4)$$

Let $u_0(x, k)$ be the solution of the problem (2.3), (2.4) for the case $c(x) \equiv 1$. Then

$$u_0(x, k) = \frac{\exp(-ik|x - x_0|)}{2ik}. \quad (2.5)$$

Our interest is in the following inverse problem:

Inverse Medium Scattering Problem (IMSP). *Let $[\underline{k}, \bar{k}] \subset (0, \infty)$ be an interval of wavenumbers k . Reconstruct the function $c(x)$, assuming that the following function $g_0(k)$ is known*

$$g_0(k) = \frac{u(0, k)}{u_0(0, k)}, k \in [\underline{k}, \bar{k}]. \quad (2.6)$$

Denote

$$w(x, k) = \frac{u(x, k)}{u_0(x, k)}. \quad (2.7)$$

It follows from (2.6), (2.7) and [32] that

$$w(0, k) = g_0(k), k \in [\underline{k}, \bar{k}], \quad (2.8)$$

$$w'(0, k) = g_1(k) = 2ik(g_0(k) - 1), k \in [\underline{k}, \bar{k}]. \quad (2.9)$$

2.2 Some properties of the solution of forward and inverse problems

In this subsection we briefly outline some results of [32], which we use below in this paper. Existence and uniqueness of the solution $u(x, k) \in C^3(\mathbb{R})$ for each $k > 0$ was established in [32]. Also, it was proven in [32] that

$$u(x, k) \neq 0, \forall x \in [0, 1], \forall k > 0. \quad (2.10)$$

In particular, $g_0(k) \neq 0, \forall k \in [\underline{k}, \bar{k}]$. In addition, uniqueness of our IMSP was proven in [32]. Also, the following asymptotic behavior of the function $u(x, k)$ takes place:

$$u(x, k) = \frac{1}{2ikc^{1/4}(x)} \exp \left[-ik \int_{x_0}^x \sqrt{c(\xi)} d\xi \right] (1 + \hat{u}(x, k)), k \rightarrow \infty, \forall x \in [0, 1], \quad (2.11)$$

$$\hat{u}(x, k) = O\left(\frac{1}{k}\right), \partial_k \hat{u}(x, k) = O\left(\frac{1}{k^2}\right), k \rightarrow \infty. \quad (2.12)$$

Given (2.10) and (2.11) we now can uniquely define the function $\log w(x, k)$ as in [32]. The difficulty here is in defining $\text{Im}(\log u(x, k))$, since this number is usually defined up to the addition of $2n\pi$, where n is an integer. For sufficiently large values of k we define the function $\log w(x, k)$ using (2.5), (2.7), (2.11) and (2.12) as

$$\log w(x, k) = -\frac{1}{4} \ln c(x) - ik \left(\int_{x_0}^x \sqrt{c(\xi)} d\xi - x + x_0 \right) + \hat{w}(x, k), x \in (0, 1), \quad (2.13)$$

where

$$\hat{w}(x, k) = O\left(\frac{1}{k}\right), \partial_k \hat{w}(x, k) = O\left(\frac{1}{k^2}\right), k \rightarrow \infty. \quad (2.14)$$

Hence, for sufficiently large k ,

$$|\hat{w}(x, k)| < 2\pi, \quad (2.15)$$

which eliminates the above mentioned ambiguity. Suppose that the number \bar{k} is so large that (2.15) is true for $k \geq \bar{k}$. Then $\log w(x, \bar{k})$ is defined as in (2.13). As to not large values of k , we define the function (2.13) = $\log w(x, k)$ as

$$\psi(x, k) = - \int_k^{\bar{k}} \frac{\partial_k w(x, \xi)}{w(x, \xi)} d\xi + \log w(x, \bar{k}). \quad (2.16)$$

By (2.10) $w(x, \xi) \neq 0, \forall x \in [0, 1], \forall \xi > 0$. Differentiating both sides of (2.16) with respect to k , we obtain

$$\partial_k w(x, k) - w(x, k) \partial_k \psi(x, k) = 0. \quad (2.17)$$

Multiplying both sides of (2.17) by $\exp(-\psi(x, k))$, we obtain $\partial_k (e^{-\psi(x, k)} w(x, k)) = 0$. Hence, there exists a function $C = C(x)$ independent on k such that

$$w(x, k) = C(x) e^{\psi(x, k)}. \quad (2.18)$$

Setting in (2.18) $k = \bar{k}$ and using the fact that by (2.16) $\psi(x, \bar{k}) = \log w(x, \bar{k})$, we obtain

$$C = C(x) = 1, x \in [0, 1]. \quad (2.19)$$

Hence, (2.16) and (2.18) imply that $\log w(x, k)$ is defined as $\log w(x, k) = \psi(x, k)$.

3 The Weighted Cost Functional

In this section we construct the above mentioned weighted cost functional with the CWF in it.

Lemma 3.1 (Carleman estimate). *For any complex valued function $u \in H^2(0, 1)$ with $u(0) = u'(0) = 0$ and for any parameter $\lambda > 1$ the following Carleman estimate holds*

$$\int_0^1 |u''|^2 e^{-2\lambda x} dx \geq C \left[\int_0^1 |u''|^2 e^{-2\lambda x} dx + \lambda \int_0^1 |u'|^2 e^{-2\lambda x} dx + \lambda^3 \int_0^1 |u|^2 e^{-2\lambda x} dx \right], \quad (3.1)$$

where the constant $C > 0$ is independent of u and λ .

Proof. In the case when the integral with u'' is absent in the right hand side of (3.1) this lemma was proved in [32]. To incorporate this integral, we note that

$$2 \int_0^1 |u''|^2 e^{-2\lambda x} dx \geq \int_0^1 |u''|^2 e^{-2\lambda x} dx + C \left[\lambda \int_0^1 |u'|^2 e^{-2\lambda x} dx + \lambda^3 \int_0^1 |u|^2 e^{-2\lambda x} dx \right]. \quad (3.2)$$

Let $\tilde{C} = \min(C/2, 1/2)$. Then (3.2) implies (3.1) where C is replaced with \tilde{C} . \square

3.1 Nonlinear integro-differential equation

For $x \in [0, 1], k \in [k, \bar{k}]$ consider the function $v(x, k)$ and its k -derivative $q(x, k)$, where

$$v(x, k) = \frac{\log w(x, k)}{k^2}, \quad q(x, k) = \partial_k v(x, k). \quad (3.3)$$

Hence,

$$v(x, k) = - \int_k^{\bar{k}} q(x, \tau) d\tau + v(x, \bar{k}). \quad (3.4)$$

Consider the function $V(x) = V(x, \bar{k})$, which we call the “tail function”, and this function is unknown,

$$V(x) = v(x, \bar{k}). \quad (3.5)$$

Let $\beta(x) = c(x) - 1$. Note that since $c(x) = 1$ for $x \geq 1$, then equation (2.3) and the first condition (2.4) imply that $u(x, k) = A(k) e^{-ikx}$ for $x \geq 1$. Hence, (2.5) and (2.7) imply that $w'(x, k) = 0$ for $x \geq 1$. It follows from (2.3), (2.5), (2.7)–(2.9), (2.18) and (2.19) that

$$w'' - 2ikw' + k^2\beta(x)w = 0, \quad x \in (0, 1), \quad (3.6)$$

$$w(0, k) = g_0(k), \quad w'(0, k) = g_1(k), \quad w'(1, k) = 0. \quad (3.7)$$

Using (2.18), (2.19), (3.3) and (3.6), we obtain

$$v'' + k^2(v')^2 - 2ikv' = -\beta(x). \quad (3.8)$$

Differentiate (3.8) with respect to k and use (3.3)–(3.7). We obtain

$$q'' - 2ikq' + 2k^2q' \left(- \int_k^{\bar{k}} q'(x, \tau) d\tau + V'(x) \right) - 2i \left(- \int_k^{\bar{k}} q'(x, \tau) d\tau + V'(x) \right)$$

$$+ 2k \left(- \int_k^{\bar{k}} q'(x, \tau) d\tau + V'(x) \right)^2 = 0, \quad x \in (0, 1), k \in (\underline{k}, \bar{k}), \quad (3.9)$$

$$q(0, k) = p_0(k), q'(0, k) = p_1(k), q'(1, k) = 0, k \in (\underline{k}, \bar{k}), \quad (3.10)$$

where

$$p_0(k) = \frac{\partial}{\partial k} \left(\frac{\log g_0(k)}{k^2} \right), p_1(k) = \frac{\partial}{\partial k} \left[\frac{2i}{k} \left(1 - \frac{1}{g_0(k)} \right) \right], k \in [\underline{k}, \bar{k}]. \quad (3.11)$$

We have obtained an integro-differential equation (3.9) for the function q with the overdetermined boundary conditions (3.10). The tail function $V(x)$ is also unknown. First, we will approximate the tail function V . Next, we will solve the problem (3.9), (3.10) for the function q . To solve this problem, we will construct the above mentioned weighted cost functional with the CWF $e^{-2\lambda x}$ in it, see (3.1). This construction, combined with corresponding analytical results, is the *central* part of our paper. Thus, even though the problem (3.9)-(3.11) is the same as the problem (65), (66) in [32], the numerical method of the solution of the problem (3.9)-(3.11) is *radically* different from the one in [32].

Now, suppose that we have obtained approximations for both functions $V(x)$ and $q(x, k)$. Then we obtain the unknown coefficient $\beta(x)$ via backwards calculations. First, we calculate the approximation for the function $v(x, k)$ via (3.4) and (3.5). Next, we calculate the function $\beta(x) = c(x) - 1$ via (3.8). We have learned from our numerical experience that the best value of k to use in (3.8) for the latter calculation is $k = \underline{k}$.

3.2 Approximation for the tail function $V(x)$

The approximation for the tail function is done here the same way as the approximation for the so-called ‘‘first tail function’’ in section 4.2 of [32]. However, while tail functions are updated in [32], we are not doing such updates here.

It follows from (2.7)-(2.14) and (3.3)-(3.5) that there exists a function $r(x) \in C^2[0, 1]$ such that

$$V(x, k) = \frac{r(x)}{k} + O\left(\frac{1}{k^2}\right), \quad q(x, k) = -\frac{r(x)}{k^2} + O\left(\frac{1}{k^3}\right), \quad k \rightarrow \infty, x \in (0, 1). \quad (3.12)$$

Hence, assuming that the number \bar{k} is sufficiently large, we drop terms $O(1/\bar{k}^2)$ and $O(1/\bar{k}^3)$ in (3.12). Next, we set

$$V(x, k) = \frac{r(x)}{k}, \quad q(x, k) = -\frac{r(x)}{k^2}, \quad k \geq \bar{k}, x \in (0, 1). \quad (3.13)$$

Set $k := \bar{k}$ in (3.9) and (3.10). Next, substitute (3.13) in (3.9) and (3.10) at $k = \bar{k}$. We obtain $r'' = 0$. Recall that functions g_0 and g_1 are linked via (2.9). Thus,

$$V'' = 0, \quad \text{in } (0, 1), \quad (3.14)$$

$$V(0) = \frac{\log g_0(\bar{k})}{\bar{k}^2}, \quad V'(0) = \frac{i}{\bar{k}} \left(1 - \frac{1}{g_0(\bar{k})} \right), \quad V'(1) = 0, \quad (3.15)$$

where functions g_0 and $g_1(k)$ are defined in (2.8) and (2.9) respectively. It seems to be at the first glance that one can find the function V as, for example Cauchy problem for ODE (3.14) with data $V(0)$ and $V'(0)$. However, it was noticed in Remark 5.1 of [34] that this approach, being applied to a similar problem, does not lead to good results. We have the same observation in our numerical studies. This is likely to the approximate nature of (3.13). Thus, just like in [32], we solve the problem (3.14), (3.15) by the Quasi-Reversibility Method (QRM). The boundary condition $V'(1) = 0$ provides a better stability property.

So, we minimize the following functional $J_\alpha(V)$ on the set W , where

$$J_\alpha(V) = \frac{1}{2} \left(\|V''\|_{L^2(0,1)}^2 + \alpha \|V\|_{H^3(0,1)}^2 \right), \quad (3.16)$$

$$V \in W := \left\{ V \in H^3(0,1) : V(0) = \frac{\log g_0(\bar{k})}{\bar{k}^2}, V'(0) = \frac{i}{\bar{k}} \left(1 - \frac{1}{g_0(\bar{k})} \right), V'(1) = 0 \right\}, \quad (3.17)$$

where $\alpha > 0$ is the regularization parameter. The existence and uniqueness of the solution of this minimization problem as well as convergence of minimizers V_α in the $H^2(0,1)$ -norm to the exact solution V^* of the problem (3.15), (3.16) with the exact data $g_0^*(\bar{k})$ as $\alpha \rightarrow 0$ were proved in [32]. We note that in the regularization theory one always assumes existence of an ideal exact solution with noiseless data [9, 17].

Recall that by the embedding theorem $H^2(0,1) \subset C^1[0,1]$ and

$$\|f\|_{C^1[0,1]} \leq C \|f\|_{H^2(0,1)}, \forall f \in H^2(0,1), \quad (3.18)$$

where $C > 0$ is a generic constant. Theorem 3.1 is a reformulation of Theorem 4.2 of [32].

Theorem 3.1. *Let the function $c^*(x)$ satisfying conditions (2.1)-(2.2) be the exact solution of our IMSP with the noiseless data $g_0^*(k) = w^*(0,k)$, $k \in [\underline{k}, \bar{k}]$, where $w^*(x,k) = u^*(x,k)/u_0(x,k)$ and $u^*(x,k)$ is the solution of the forward problem (2.3), (2.4). Let the exact tail function $V^*(x, \bar{k}) = \bar{k}^{-2} \log w^*(x, \bar{k})$ and the function $q^*(x, \bar{k}) = \partial_k V^*(x, k)|_{k=\bar{k}}$ have the form (3.13) with $r := r^*(x)$. Assume that for $k \in [\underline{k}, \bar{k}]$*

$$|\log g_0(k) - \log g_0^*(k)| \leq \delta, |g_0(k) - g_0^*(k)| \leq \delta, |g_0'(k) - (g_0^*)'(k)| \leq \delta, \quad (3.19)$$

where $\delta > 0$ is a sufficiently small number, which characterizes the level of the error in the boundary data. Let in (3.16) $\alpha = \alpha(\delta) = \delta^2$. Let the function $V_{\alpha(\delta)}(x) \in H^3(0,1)$ be the minimizer of the functional (3.16) on the set of functions W defined in (3.17). Then there exists a constant $C_1 = C_1(\bar{k}, c^*) > 0$ depending only on \bar{k} and c^* such that

$$\|V_{\alpha(\delta)}(x) - V^*(x, \bar{k})\|_{C^1[0,1]} \leq C \|V_{\alpha(\delta)}(x) - V^*(x, \bar{k})\|_{H^2(0,1)} \leq C_1 \delta. \quad (3.20)$$

Remark 3.1. We have also tried to consider two terms in the asymptotic expansion for V in (3.12): the second one with $1/k^2$. This resulted in a nonlinear system of two equations. We have solved it by via minimizing an analog of the functional of section 3.3. However, the quality of resulting images deteriorated as compared with the above function $V_{\alpha(\delta)}(x)$. In addition, we have tried to iterate with respect to the tail function V . However, the quality of resulting images has also deteriorated.

3.3 The weighted cost functional

Consider the function $q(x, k)$ satisfying (3.9)-(3.11). In sections 5.2 and 5.3 we use Lemma 2.1 and Theorem 2.1 of [4]. To apply theorems, we need to have zero boundary conditions at $x = 0, 1$. Hence, we introduce the function $p(x, k)$,

$$p(x, k) = q(x, k) - (x^2 - 1)^2 p_0 - x(x^2 - 1)^2 p_1, \text{ where } p_0 = p_0(k), p_1 = p_1(k). \quad (3.21)$$

Denote

$$m(x, k) = (x^2 - 1)^2 p_0(k) + x(x^2 - 1)^2 p_1(k). \quad (3.22)$$

Also, replace in (3.9) V with $V_{\alpha(\delta)}$. Then (3.9), (3.10) and (3.21) and (3.22) imply that

$$\begin{aligned} L(p) = p'' + m'' - 2ik(p' + m') + 2k^2(p' + m') & \left(- \int_k^{\bar{k}} (p' + m')(x, \tau) d\tau + V'_{\alpha(\delta)}(x) \right) \\ - 2i & \left(- \int_k^{\bar{k}} (p' + m')(x, \tau) d\tau + V'(x) \right) + 2k \left(- \int_k^{\bar{k}} (p' + m')(x, \tau) d\tau + V'_{\alpha(\delta)}(x) \right)^2 = 0 \end{aligned} \quad (3.23)$$

$$p(0, k) = 0, p'(0, k) = 0, p'(1, k) = 0. \quad (3.24)$$

Introduce the Hilbert space H of pairs of real valued functions $f(x, k) = (f_1(x, k), f_2(x, k))$, $(x, k) \in (0, 1) \times (\underline{k}, \bar{k})$ as

$$H = \left\{ \begin{array}{l} f(x, k) : f(0, k) = f'(0, k) = f'(1, k) = 0, \\ \|f\|_H = \left[\int_{\underline{k}}^{\bar{k}} \|f(x, k)\|_{H^2(0,1)}^2 dk \right]^{1/2} < \infty \end{array} \right\}. \quad (3.25)$$

Here and below $\|f(x, k)\|_{H^2(0,1)}^2 = \|f_1(x, k)\|_{H^2(0,1)}^2 + \|f_2(x, k)\|_{H^2(0,1)}^2$.

Based on (3.23) and (3.24), we define our weighted cost functional as

$$J_\lambda(p) = e^{2\lambda} \int_{\underline{k}}^{\bar{k}} \int_0^1 |L(p)|^2 e^{-2\lambda x} dx dk, \forall p \in H. \quad (3.26)$$

Let $R > 0$ be an arbitrary number. Let $\overline{B(R)}$ be the closure in the norm of the space H of the open set $B(R) \subset H$ of functions $p(x, k)$ defined as

$$B(R) = \{p \in H : \|p\|_H < R\}. \quad (3.27)$$

Minimization Problem. *Minimize the functional $J_\lambda(p)$ on the set $\overline{B(R)}$.*

Remark 3.1. The analytical part of this paper below is dedicated to this minimization problem. Since we deal with complex valued functions, we consider below $J_\lambda(p)$ as the functional with respect to the 2-D vector of real valued functions $p(x, k) = (\text{Re } p(x, k), \text{Im } p(x, k)) = (p_1(x, k), p_2(x, k)) \in H$. Thus, even though we consider complex conjugations below, this is done only for the convenience of writing. Below $[\cdot, \cdot]$ is the scalar product in H . Even though we use in (3.21) and (3.23) the functions $p_0 = p_0(k)$, $p_1 = p_1(k)$, it is always clear from the context below what do we actually mean in each particular case: the first component of $p_1(x, k)$ of the vector function $p(x, k)$ or the above functions $p_0(k)$, $p_1(k)$.

4 The Global Strict Convexity of $J_\lambda(p)$

Theorem 4.1 is the main analytical result of this paper.

Theorem 4.1. *Assume that conditions of Theorem 3.1 are satisfied. Then the functional $J_\lambda(p)$ has the Frechét derivative $J'_\lambda(p)$ for all $p \in H$. Also, there exists a sufficiently large number $\lambda_0 = \lambda_0(r^*, \underline{k}, \bar{k}, \|p_1\|_{C[\underline{k}, \bar{k}]}, R) > 1$ depending only on listed parameters and a generic constant $C > 0$, such that for all $\lambda \geq \lambda_0$ the functional $J_\lambda(p)$ is strictly convex on $\overline{B(R)}$, i.e. for all $p, p+h \in \overline{B(R)}$*

$$J_\lambda(p+h) - J_\lambda(p) - J'_\lambda(p)(h) \geq C \|h\|_H^2. \quad (4.1)$$

Proof. Everywhere below in this paper $C_2 = C_2(r^*, \underline{k}, \bar{k}, \|p_1(k)\|_{C[\underline{k}, \bar{k}]}, R) > 0$ denotes different constants depending only on listed parameters. Since conditions of Theorem 3.1 are satisfied, then by (3.20)

$$\|V_{\alpha(\delta)}\|_{C^1[0,1]} \leq \|V^*\|_{C^1[0,1]} + C_1\delta \leq C_2. \quad (4.2)$$

Let $h = (h_1, h_2)$, where $h_1 = \operatorname{Re} h, h_2 = \operatorname{Im} h$. Then (3.18), (3.25) and (3.27) imply that

$$\int_{\underline{k}}^{\bar{k}} \|h(x, k)\|_{C^1[0,1]}^2 dk \leq C_2. \quad (4.3)$$

Using (4.3), we obtain

$$\begin{aligned} \left| \int_{\underline{k}}^{\bar{k}} h'(x, k) dk \right|^2 &\leq (\bar{k} - \underline{k}) \int_{\underline{k}}^{\bar{k}} |h'(x, k)|^2 dk \\ &\leq (\bar{k} - \underline{k}) \int_{\underline{k}}^{\bar{k}} \|h(x, k)\|_{C^1[0,1]}^2 dk \leq C_2. \end{aligned} \quad (4.4)$$

We use the formula

$$|a|^2 - |b|^2 = (a-b)\bar{a} + (\bar{a}-\bar{b})b, \forall a, b \in \mathbb{C}, \quad (4.5)$$

where \bar{z} is the complex conjugate of $z \in \mathbb{C}$. Denote

$$a = L(p+h), b = L(p), \quad (4.6)$$

Consider functions $A(x, k), A_1(x, k), A_2(x, k)$ defined as

$$A = |L(p+h)|^2 - |L(p)|^2, A_1(x, k) = (a-b)\bar{a}, A_2(x, k) = (\bar{a}-\bar{b})b. \quad (4.7)$$

First, using (3.23) and (4.7), we single out in A the part, which is linear with respect to the vector function $h = (h_1, h_2)$. Then

$$a = (p+h)'' + m' - 2ik(p' + h' + m')$$

$$+ 2k^2 (p' + h' + m') \left(- \int_k^{\bar{k}} (p' + h' + m') (x, \tau) d\tau + V'_{\alpha(\delta)} (x) \right) \quad (4.8)$$

$$- 2i \left(- \int_k^{\bar{k}} (p' + h' + m') (x, \tau) d\tau + V'_{\alpha(\delta)} (x) \right) + 2k \left(- \int_k^{\bar{k}} (p' + h' + m') (x, \tau) d\tau + V'_{\alpha(\delta)} (x) \right)^2.$$

By (4.7)

$$\begin{aligned} A_1(x, k) &= (a - b) \bar{a} = \left\{ h'' - \left[2ik + 2k^2 \left(\int_k^{\bar{k}} (p' + m') (x, \tau) d\tau + V'_{\alpha(\delta)} (x) \right) \right] h' \right\} \bar{a} \\ &+ \left[2k^2 (p' + m') + 2i - 4k \left(\int_k^{\bar{k}} (p' + m') (x, \tau) d\tau - V'_{\alpha(\delta)} (x) \right) \right] \int_k^{\bar{k}} h' (x, \tau) d\tau \cdot \bar{a} \quad (4.9) \\ &+ \left[-2k^2 h' \int_k^{\bar{k}} h' (x, \tau) d\tau + 2k \left(\int_k^{\bar{k}} h' (x, \tau) d\tau \right)^2 \right] \bar{a}. \end{aligned}$$

Hence,

$$\begin{aligned} A_1(x, k) &= h'' \overline{L(p)} - \left[2ik + 2k^2 \left(\int_k^{\bar{k}} (p' + m') (x, \tau) d\tau - V'_{\alpha(\delta)} (x) \right) \right] \overline{L(p)} h' \\ &+ \left[(p' + m') + 2i - 4k \left(\int_k^{\bar{k}} (p' + m') (x, \tau) d\tau - V'_{\alpha(\delta)} (x) \right) \right] \overline{L(p)} \int_k^{\bar{k}} h' (x, \tau) d\tau \quad (4.10) \\ &+ |h''(x, k)|^2 + \tilde{A}_{1,p}(h)(x, k), \end{aligned}$$

where $\tilde{A}_{1,p}(h)(x, k)$ depends nonlinearly on the vector function $(h_1, h_2)(x, k)$. Also, by (4.2)-(4.4) and the Cauchy-Schwarz inequality

$$\left| \tilde{A}_{1,p}(h) \right| (x, k) \leq \frac{1}{2} |h''(x, k)|^2 + C_2 \left(|h'(x, k)|^2 + \int_k^{\bar{k}} |h'(x, \tau)|^2 d\tau \right). \quad (4.11)$$

To explain the presence of the multiplier “1/2” at $|h''(x, k)|^2$ in (4.11), we note that it follows from (4.8) that the term $h''\bar{a}$ in (4.9) contains the term $|h''|^2$, which is included in (4.10) already, as well as terms

$$h'' \overline{h'}, \quad h'' \int_k^{\bar{k}} \overline{h'}(x, \tau) d\tau, \quad h'' \left(\int_k^{\bar{k}} \overline{h'}(x, \tau) d\tau \right)^2. \quad (4.12)$$

We now show how do we estimate the third term in (4.12), since estimates of two other terms are simpler. We use the so-called ‘‘Cauchy-Schwarz inequality with ε ’’,

$$-|(c, d)| \geq -\frac{\varepsilon}{2}|c|^2 - \frac{1}{2\varepsilon}|d|^2, \forall c, d \in \mathbb{R}^n, \forall \varepsilon > 0,$$

where $(,)$ is the scalar product in \mathbb{R}^n . Hence,

$$-\left| h'' \left(\int_k^{\bar{k}} \bar{h}'(x, \tau) d\tau \right) \right|^2 \geq -\frac{\varepsilon}{2}|h''|^2 - \frac{(\bar{k} - \underline{k})}{2\varepsilon} \int_{\underline{k}}^{\bar{k}} |h'(x, \tau)|^2 d\tau.$$

Thus, choosing appropriate numbers $\varepsilon > 0$, we obtain the term $|h''(x, k)|^2/2$ in (4.11). The second term in the right hand side of (4.11) is obtained similarly.

Analogously, using (4.5)-(4.7), we obtain

$$\begin{aligned} A_2(x, k) &= (\bar{a} - \bar{b}) b = \left\{ h'' - \left[2ik + 2k^2 \left(\int_k^{\bar{k}} (p' + m')(x, \tau) d\tau - V'_{\alpha(\delta)}(x) \right) \right] h' \right\} \cdot L(p) \\ &+ \left[(p' + m') + 2i - 4k \left(\int_k^{\bar{k}} (p' + m')(x, \tau) d\tau - V'_{\alpha(\delta)}(x) \right) \right] \int_k^{\bar{k}} h'(x, \tau) d\tau \cdot L(p) \\ &+ \tilde{A}_{2,p}(h)(x, k), \end{aligned} \quad (4.13)$$

where $\tilde{A}_{2,p}(h)(x, k)$ depends nonlinearly on the vector function $h = (h_1, h_2)$ and similarly with (4.11)

$$\left| \tilde{A}_{2,p}(h) \right|(x, k) \leq C_2 \left(|h'(x, k)|^2 + \int_{\underline{k}}^{\bar{k}} |h'(x, k)|^2 dk \right). \quad (4.14)$$

It is clear from (4.7), (4.10)-(4.14) that the linear with respect to the vector function $h = (h_1, h_2)$ part of A consists of the sum of the first two lines of (4.10) with the first two lines of (4.13). We denote this linear part as $D_p(h)(x, k)$. Then

$$A(x, k) = A_1(x, k) + A_2(x, k) = D_p(h)(x, k) + \tilde{A}_{1,p}(h)(x, k) + \tilde{A}_{2,p}(h)(x, k).$$

Thus, using (3.26) and (4.7), we obtain

$$\begin{aligned} J_\lambda(p+h) - J_\lambda(p) &= e^{2\lambda} \int_{\underline{k}}^{\bar{k}} \int_0^1 D_p(h)(x, k) e^{-2\lambda x} dx dk \\ &+ e^{2\lambda} \int_{\underline{k}}^{\bar{k}} \int_0^1 \left(\tilde{A}_{1,p}(h)(x, k) + \tilde{A}_{2,p}(h)(x, k) \right) e^{-2\lambda x} dx dk. \end{aligned} \quad (4.15)$$

Consider the expression $\tilde{D}_{p,\lambda}(h)$,

$$\tilde{D}_{p,\lambda}(h) = e^{2\lambda} \int_{\underline{k}}^{\bar{k}} \int_0^1 D_p(h)(x, k) e^{-2\lambda x} dx dk. \quad (4.16)$$

It follows from (3.23), (4.2), (4.10) and (4.13) that $\tilde{D}_{p,\lambda}(h) : H \rightarrow \mathbb{R}$ is a bounded linear functional. Hence, by Riesz theorem, there exists unique element $M_{p,\lambda} \in H$ such that

$$\tilde{D}_{p,\lambda}(h) = [M_{p,\lambda}, h], \forall h \in H. \quad (4.17)$$

It follows from (4.11) and (4.14)-(4.17) that

$$J_\lambda(p+h) - J_\lambda(p) - [M_{p,\lambda}, h] = O(\|h\|_H^2).$$

Thus, the Frechét derivative $J'_\lambda(p) \in H$ of the functional $J_\lambda(p)$ at the point p exists and

$$J'_\lambda(p) = M_{p,\lambda}. \quad (4.18)$$

Note that

$$e^{2\lambda} e^{-2\lambda x} \geq 1, \forall x \in [0, 1]. \quad (4.19)$$

Hence, using (4.11), (4.14)-(4.18) and Lemma 3.1, we obtain

$$\begin{aligned} J_\lambda(p+h) - J_\lambda(p) - J'_\lambda(p)(h) &\geq \\ &\frac{e^{2\lambda}}{2} \int_{\underline{k}}^{\bar{k}} \int_0^1 |h''|^2(x, k) e^{-2\lambda x} \\ &\quad - C_2 e^{2\lambda} \int_{\underline{k}}^{\bar{k}} \int_0^1 |h'|^2(x, k) e^{-2\lambda x} \\ &\geq C e^{2\lambda} \left[\int_0^1 |h''|^2 e^{-2\lambda x} dx + \lambda \int_0^1 |h'|^2 e^{-2\lambda x} dx + \lambda^3 \int_0^1 |h|^2 e^{-2\lambda x} dx \right] \\ &\quad - C_2 e^{2\lambda} \int_{\underline{k}}^{\bar{k}} \int_0^1 |h'|^2(x, k) e^{-2\lambda x}. \end{aligned} \quad (4.20)$$

Choose the number $\lambda_0 = \lambda_0(r^*, \underline{k}, \bar{k}, \|p_1(k)\|_{C[\underline{k}, \bar{k}]}, R) > 1$ so large that $C\lambda_0 > 2C_2$. Then, using (4.19) and (4.20), we obtain with a new generic constant $C > 0$ for all $\lambda \geq \lambda_0$

$$J_\lambda(p+h) - J_\lambda(p) - J'_\lambda(p)(h) \geq C \|h\|_H^2. \quad \square$$

5 Global Convergence of the Gradient Projection Method

Using Theorem 4.1, we establish in this section the global convergence of the gradient projection method of the minimization of the functional $J_\lambda(p)$. As to some other versions of the gradient method, they will be discussed in follow up publications.

5.1 Lipschitz continuity of $J'_\lambda(p)$ with respect to p

First, we need to prove the Lipschitz continuity of the functional $J'_\lambda(p)$ with respect to p .

Theorem 5.1. *Let conditions of Theorem 3.1 hold. Then the functional $J'_\lambda(p)$ is Lipschitz continuous on the closed ball $\overline{B(R)}$. In other words,*

$$\|J'_\lambda(p^{(1)}) - J'_\lambda(p^{(2)})\|_H \leq C_2 e^{2\lambda} \|p^{(1)} - p^{(2)}\|_H, \forall p^{(1)}, p^{(2)} \in \overline{B(R)}, \forall \lambda > 0. \quad (5.1)$$

Proof. Consider, for example the first line of (4.10) for $p = p^{(1)}$ and denote it $A_{1,1}(x, k)(p^{(1)}, h)$. We define $A_{1,1}(x, k)(p^{(2)}, h)$ similarly. Both these expressions are linear with respect to $h = (h_1, h_2)$. Denote $\tilde{p} = p^{(1)} - p^{(2)}$. We have

$$\begin{aligned} & A_{1,1}(x, k)(p^{(1)}, h) - A_{1,1}(x, k)(p^{(2)}, h) = \\ & \left(\overline{L(p^{(1)})} - \overline{L(p^{(2)})} \right) \left[h'' - \left(2ik + 2k^2 \left(\int_k^{\bar{k}} (p^{(1)} + m)'(x, \tau) d\tau - V'_{\alpha(\delta)}(x) \right) \right) h' \right] \\ & \quad - 2k^2 \left[\overline{L(p^{(2)})} \int_k^{\bar{k}} \tilde{p}'(x, \tau) d\tau \right] h'. \end{aligned} \quad (5.2)$$

It is clear from (3.23) that $\left| \overline{L(p^{(1)})} - \overline{L(p^{(2)})} \right| \leq C_2 (|\tilde{p}''| + |\tilde{p}'|)$. Hence, using (4.19), (5.2) and Cauchy-Schwarz inequality, we obtain

$$\begin{aligned} & \left| e^{2\lambda} \int_{\underline{k}}^{\bar{k}} \int_0^1 (A_{1,1}(x, k)(p^{(1)}, h) - A_{1,1}(x, k)(p^{(2)}, h)) e^{-2\lambda x} dx dk \right| \\ & \leq C_2 e^{2\lambda} \|p^{(1)} - p^{(2)}\|_H \|h\|_H. \end{aligned}$$

The rest of the proof of (5.1) is similar. \square

5.2 The minimizer of $J_\lambda(p)$ on the set $\overline{B(R)}$

Theorem 5.2 claims the existence and uniqueness of the minimizer of the functional $J_\lambda(p)$ on the set $\overline{B(R)}$.

Theorem 5.2. *Let conditions of Theorem 4.1 hold. Then for every $\lambda \geq \lambda_0$ there exists unique minimizer $p_{\min, \lambda}$ of the functional $J_\lambda(p)$ on the set $\overline{B(R)}$. Furthermore,*

$$[J'(p_{\min, \lambda}), y - p_{\min, \lambda}] \geq 0, \forall y \in \overline{B(R)}. \quad (5.3)$$

Proof. This theorem follows immediately from the above Theorem 4.1 and Lemma 2.1 of [4]. \square

Let $Q_{\overline{B}} : H \rightarrow \overline{B(R)}$ be the operator of the projection of the space H on the closed ball $\overline{B(R)}$. Let $\gamma = \text{const.} > 0$ and let $p^{(0)}$ be an arbitrary point of $\overline{B(R)}$. Consider the sequence of the gradient projection method,

$$p^{(n+1)} = Q_{\overline{B}}(p^{(n)} - \gamma J'_\lambda(p^{(n)})), n = 0, 1, \dots \quad (5.4)$$

Theorem 5.3. *Let conditions of Theorem 4.1 hold. Then for every $\lambda \geq \lambda_0$ there exists a sufficiently small number $\gamma_0 = \gamma_0 \left(r^*, \underline{k}, \bar{k}, \|p_0\|_{C[\underline{k}, \bar{k}]}, \|p_1\|_{C[\underline{k}, \bar{k}]}, R, \lambda \right) \in (0, 1)$ and a number $q = q(\gamma) \in (0, 1)$ such that for every $\gamma \in (0, \gamma_0)$ the sequence (5.4) converges to the unique minimizer $p_{\min, \lambda}$ of the functional $J_\lambda(p)$ on the set $\overline{B(R)}$ and*

$$\|p^{(n)} - p_{\min, \lambda}\|_H \leq q^n(\gamma) \|p^{(0)} - p_{\min, \lambda}\|_H, n = 1, \dots \quad (5.5)$$

Proof. This theorem follows immediately from the above Theorem 4.1 and Theorem 2.1 of [4]. \square

5.3 Global convergence of the gradient projection method

As it was pointed out in section 3.2, following one of the main concepts of the regularization theory [9, 17], we assume the existence of the exact solution $c^*(x)$ of our IMSP with the exact, i.e. noiseless, data $g_0^*(k)$ in (2.6). Below the superscript “*” denotes quantities generated by $c^*(x)$. The level of the error $\delta > 0$ was introduced in our data in (3.19). In particular, it follows from (3.10), (3.11) and (3.19) that

$$\|p_0 - p_0^*\|_{C[\underline{k}, \bar{k}]}, \|p_1 - p_1^*\|_{C[\underline{k}, \bar{k}]} \leq C_3 \delta, \quad (5.6)$$

where the number $C_3 = C_3(\underline{k}, \bar{k}) > 0$ depends only on listed parameters. Thus, in this section we show that the gradient projection method delivers points in a small neighborhood of the function p^* and, therefore, of the function c^* . The size of this neighborhood is proportional to δ . It is convenient to indicate in this section dependencies of the functional J_λ from p_0, p_1 and V . Hence we write in this section $J_\lambda(p, p_0, p_1, V_{\alpha(\delta)})$.

Theorem 5.4. *Assume that conditions of Theorem 4.1 hold. Also, let the exact function $p^* \in B(R)$. Then the following accuracy estimates hold for each $\lambda \geq \lambda_0$*

$$\|p_{\min, \lambda} - p^*\|_H \leq C_2 \delta, \quad (5.7)$$

$$\|c_{\min, \lambda} - c^*\|_{L_2(0,1)} \leq C_2 \delta, \quad (5.8)$$

where $p_{\min, \lambda}$ is the minimizer of the functional $J_\lambda(p, p_0, p_1, V_{\alpha(\delta)})$, which is guaranteed by Theorem 5.2 and $c_{\min, \lambda}$ is the corresponding reconstructed coefficient (section 3.1). In addition, let $\{p^{(n)}\}_{n=0}^\infty \subset \overline{B(R)}$ be the sequence (5.4) of the gradient projection method, where p_0 is an arbitrary point of $\overline{B(R)}$ and numbers $\gamma_0, \gamma \in (0, \gamma_0)$ and $q(\gamma)$ are the same as in Theorem 5.3. Let $\{c_n\}_{n=0}^\infty$ be the corresponding sequence of reconstructed coefficients (section 3.1). Then the following estimates hold

$$\|p^{(n)} - p^*\|_H \leq C_2 \delta + q^n(\gamma) \|p_0 - p_{\min, \lambda}\|_H, n = 1, \dots, \quad (5.9)$$

$$\|c_n - c^*\|_{L_2(0,1)} \leq C_2 \delta + C_2 q^n(\gamma) \|p_0 - p_{\min, \lambda}\|_H, n = 1, \dots \quad (5.10)$$

Proof. Obviously

$$J_\lambda(p^*, p_0^*, p_1^*, V^*) = 0. \quad (5.11)$$

Using (3.20), (3.22), (3.23), (5.6) and (5.11), we obtain

$$J_\lambda(p^*, p_0, p_1, V_{\alpha(\delta)}) = J_\lambda(p^*, p_0^* + (p_0 - p_0^*), p_1^* + (p_1 - p_1^*), V^* + (V_{\alpha(\delta)} - V^*))$$

$$\begin{aligned} &\leq J_\lambda(p^*, p_0^*, p_1^*, V^*) + C_2 \left[|p_0 - p_0^*| + |p_1 - p_1^*| + |(V_{\alpha(\delta)} - V^*)| \right] J_\lambda(p^*, p_0^*, p_1^*, V^*) \quad (5.12) \\ &\quad + C_2 \left(\|p_0 - p_0^*\|_{C[\underline{k}, \bar{k}]}^2 + \|p_1 - p_1^*\|_{C[\underline{k}, \bar{k}]}^2 + \|V_{\alpha(\delta)} - V^*\|_{C^1[0,1]}^2 \right) \leq C_2 \delta^2. \end{aligned}$$

By Theorems 4.1 and 5.2

$$\begin{aligned} J_\lambda(p^*, p_0, p_1, V_{\alpha(\delta)}) - J_\lambda(p_{\min, \lambda}, p_0, p_1, V_{\alpha(\delta)}) - [J'_\lambda(p_{\min, \lambda}, p_0, p_1, V_{\alpha(\delta)}), p^* - p_{\min, \lambda}] \quad (5.13) \\ \geq C \|p_{\min, \lambda} - p^*\|_H^2. \end{aligned}$$

By (5.3) and (5.12)

$$- [J'_\lambda(p_{\min, \lambda}, p_0, p_1, V_{\alpha(\delta)}), p^* - p_{\min, \lambda}] \leq 0, \quad J_\lambda(p^*, p_0, p_1, V_{\alpha(\delta)}) \leq C_2 \delta^2.$$

Hence, (5.13) implies (5.7). Since the function $c_{\min, \lambda}$ is obtained from the functions $p_{\min, \lambda}$ and $V_{\alpha(\delta)}$ as described in the end of section 3.1, then (5.7) implies (5.8). Next, (5.9) follows from (5.5) and (5.7). Finally, (5.10) follows from that procedure of section 3.1 and (5.8). \square

Remark 5.1. Therefore, Theorem 5.4 ensures the global convergence property of our method, see the definition in Introduction.

6 Numerical Studies

Since the theory of sections 3-5 is the main focus of this paper, we omit some details of the numerical implementation, both in this and next sections.

6.1 Algorithm

We now briefly describe our numerical steps for both computationally simulated and experimental data.

To minimize the functional $J_\lambda(p)$, we have written the derivatives of the operator $L(p)$ via finite differences with the step size $h_x = 0.02$. Also, we have written integrals with respect to k in discrete forms, using the trapezoidal rule, with the step size $h_k = 0.1$. The differentiation of the data $g_0(k)$ with respect to k , which we need in our method (see (3.11)), was performed using finite differences with the step size $h_k = 0.1$. We have not observed any instabilities after the differentiation, probably because the number h_k is not too small. Similar conclusions were drawn in works [8, 9, 10, 15, 29, 31, 32, 33, 34, 35, 39, 48] where similar differentiations were performed, including cases with experimental data

Next, we have minimized the corresponding discrete version of $J_\lambda(p)$ with respect to the values of the function $p(x, k)$ at those grid points. Initially we have used the gradient projection method. However, we have observed in our computations that the regular and simpler gradient method provides practically the same results. Hence, all computational results below are obtained via the gradient method. The starting point of this method was $p^{(0)} \equiv 0$ and a specific ball $B(R)$ was not used. The latter means that computational results are less pessimistic ones than our theory is. The step size of the gradient method $\gamma = 10^{-5}$ was used. We have observed that this step size is the optimal one for our computations. The computations were stopped after 5000 iterations.

Based on our above theory, we have developed the following algorithm:

1. Find the tail function $V(x)$ via minimizing the functional (3.16).
2. Minimize the functional (3.26). Let $p_{\min,\lambda}(x, k)$ be its minimizer.
3. Calculate the function $q_{\min,\lambda}(x, k) = p_{\min,\lambda}(x, k) + m(x, k)$, see (3.21) and (3.22).
4. Compute

$$v(x, \underline{k}) = - \int_{\underline{k}}^{\bar{k}} q(x, \tau) d\tau + V(x).$$

5. Compute the function $\tilde{c}_{comp}(x)$, see (2.1) and (3.8),

$$\tilde{c}_{comp}(x) = \left| -v''(x, \underline{k}) - \underline{k}^2 (v'(x, \underline{k}))^2 + 2i\underline{k}v'(x, \underline{k}) \right| + 1. \quad (6.1)$$

In this algorithm, unlike the previous globally convergent algorithms, [8, 9, 15, 31, 32, 34, 35, 39, 48], we do not need to update the tail function $V(x)$.

6.2 Numerical testing of computationally simulated data

First, we reconstruct the spatially distributed dielectric constant from computationally simulated data, which is generated by solving the problem (2.3), (2.4) via the 1-D analog of the Lippmann-Schwinger equation [32]:

$$u(x, k) = \frac{\exp(-ik|x - x_0|)}{2ik} + k^2 \int_0^1 \frac{\exp(-ik|x - \xi|)}{2ik} (c(\xi) - 1)u(\xi, k) d\xi.$$

Here and thereafter, we have use $x_0 = -1$ in all our computations. Keeping in mind our desired application to imaging of flash explosive-like targets, we have chosen in our numerical experiments the true test coefficient $c_{true}(x)$ as:

$$c_{true}(x) = \begin{cases} 7, & x \in (x_{loc} - d/2, x_{loc} + d/2), \\ 1, & \text{elsewhere,} \end{cases} \quad (6.2)$$

where x_{loc} is the location of the center of our target of interest and d is its width. Hence, the inclusion/background contrast in (6.2) is 7. For our numerical experiments we have chosen in (6.2)

$$x_{loc} = 0.1, 0.2, 0.3, 0.4 \text{ and } d = 0.1. \quad (6.3)$$

Figure 1 displays a typical behavior of the modulus of the simulated data $|u(0, k)|$ at the measurement point $x = 0$. One can observe that

$$|u(0, k)| \approx 0 \text{ for } k > 2. \quad (6.4)$$

Next, $|u(0, k)|$ changes too rapidly for $k < 0.5$. Hence, the interval $k \in [0.5, 1.5]$ seems to be the optimal one, and we indeed observed this in our computations. Hence, we choose for our study $\underline{k} = 0.5$ and $\bar{k} = 1.5$. We note that even though the above theory of the choice of the tail function $V(x)$ works only for sufficiently large values of \bar{k} , the notion “sufficiently large” is relative, see, e.g. (6.4). Besides, it is clear from section 7 that we actually work in the Gigahertz range of frequencies, and this can be considered as the range of large frequencies in Physics.

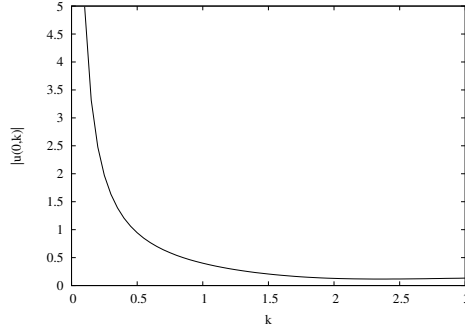


Figure 1: The modulus of simulated data on the measurement point $|u(0, k)|$

Next, having the values of $u(0, k)$, we calculate the function $g_0(k)$ in (2.6) and introduce the random noise in this function

$$g_{0,noise}(k) = g_0(k)(1.0 + 0.05 \sigma(k)), \quad \sigma(k) = \sigma_1(k) + i\sigma_2(k),$$

where $\sigma_1(k)$ and $\sigma_2(k)$ are random numbers, uniformly distributed on $(-1, 1)$.

The next important question is about the choice of an optimal parameter $\lambda = \lambda_{opt}$. Indeed, even though Theorem 4.1 says that the functional $J_\lambda(p)$ is strictly convex on the closed ball $\overline{B(R)}$ for all $\lambda \geq \lambda_0$, in fact, the larger λ is, the less is the influence on $J_\lambda(p)$ of those points $x \in (0, 1)$, which are relatively far from the point $\{x = 0\}$ where the data are given. Hence, we need to choose such a value of λ_{opt} , which would provide us satisfactory images of inclusions, whose centers x_{loc} are as in (6.3): $x_{loc} \in [0.1, 0.4]$.

Let $\|\nabla J_\lambda(p)\|_{L_2((0,1) \times (\underline{k}, \overline{k}))}$ be the discrete $L_2((0, 1) \times (\underline{k}, \overline{k}))$ – norm of the gradient of the above described discrete version of the functional $J_\lambda(p)$. Figure 2 displays the dependencies of this norm on the number of iteration of the gradient method for different values of λ . We have observed in our computations that these dependencies are very similar for targets satisfying (6.2), (6.3) with different values of target/background contrasts. One can see that the process diverges at $\lambda = 0$, which is to be expected, since convexity of $J_{\lambda=0}(p)$ is not guaranteed. Also, we observe that the larger λ is, the faster the process converges. We have found that the optimal value of λ for targets satisfying (6.3) is $\lambda_{opt} = 3$.

We also apply a post-processing procedure after step 5 of the above algorithm. More precisely, we smooth out the function $\tilde{c}_{comp}(x)$ (6.1) using a simple averaging procedure over two neighboring grid points. Next, the resulting function $\hat{c}_{comp}(x)$ is truncated as

$$c_{comp}(x) = \begin{cases} \hat{c}_{comp}(x), & \text{if } \hat{c}_{comp}(x) \geq 0.8 \max(\hat{c}_{comp}(x)), \\ 1, & \text{otherwise.} \end{cases} \quad (6.5)$$

The function $c_{comp}(x)$ in (6.5) is considered as our reconstructed coefficient $c(x)$.

The computational results c_{comp} for different values of x_{loc} are shown in Figure 3. One can see that the proposed algorithm accurately reconstructs both locations and values of the coefficient $c_{true}(x)$. Similar accuracy was obtained for other target/background contrasts in (6.2) varying from 2 to 10.

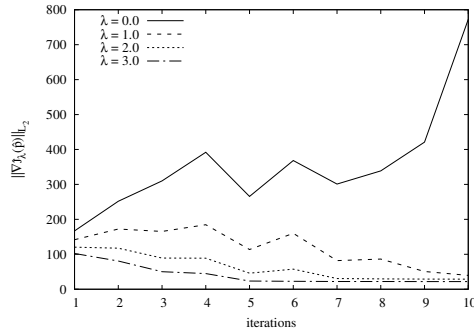


Figure 2: The discrete L_2 norm of the gradient of the functional $J_\lambda(p)$ for different λ

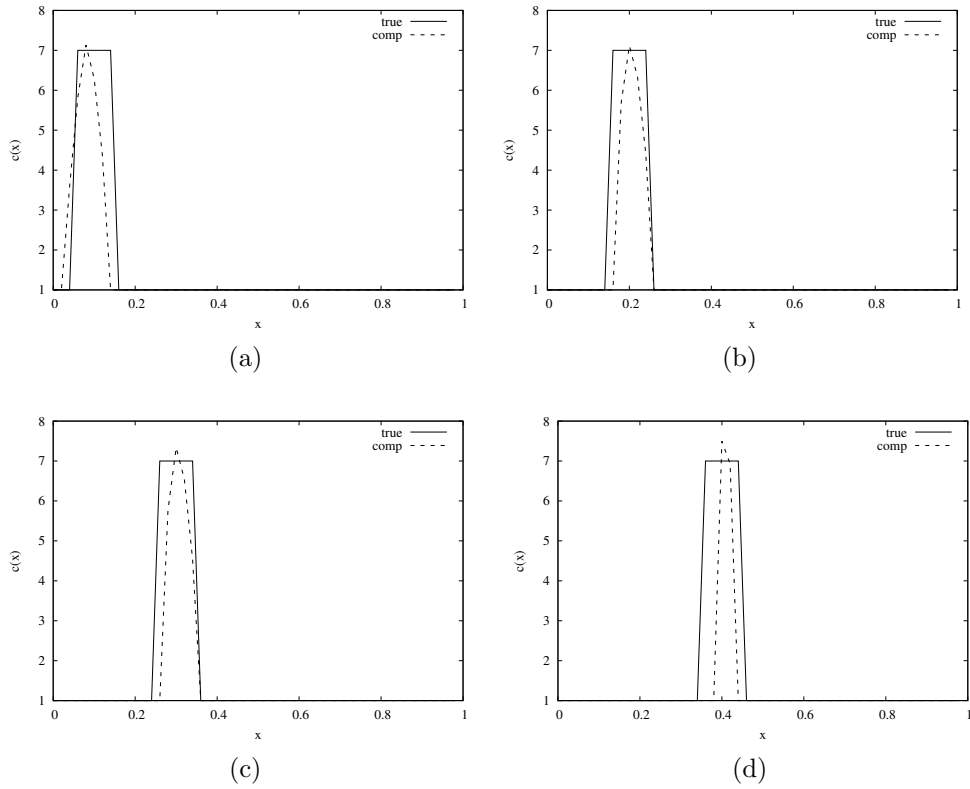


Figure 3: True (solid line) and computed (dashed line) coefficients $c(x)$. a) $x_{loc} = 0.1$, b) $x_{loc} = 0.2$, c) $x_{loc} = 0.3$, d) $x_{loc} = 0.4$. The optimal value $\lambda_{opt} = 3$ was used in all computations.

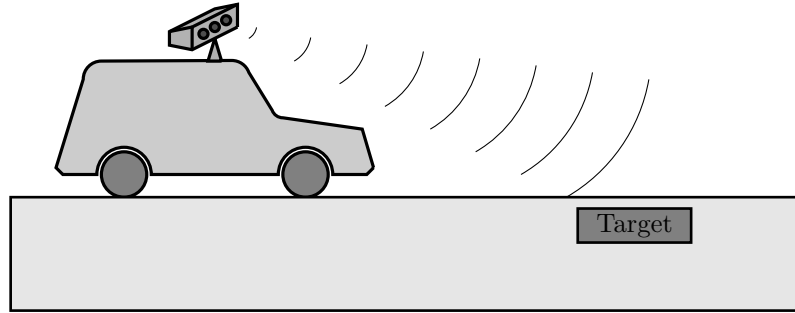


Figure 4: Schematic diagram of data collection by the Forward Looking Radar of the US Army Research Laboratory

7 Numerical Results for Experimental Data

We use here the same experimental data as ones used in [32, 34, 35], where these data were treated by the tail functions method. Thus, it is worth to test the new method of this paper on the same data set. In [34, 35] the wave propagation process was modeled by a 1-D hyperbolic equation, the Laplace transform with respect to time was applied to the solution of this equation and then the tail functions method was applied to the corresponding IMSP. In [32] the process was modeled by IMSP (2.6) and the tail functions method was applied to this IMSP. The data in [34, 35] and in [32] were obtained after applying Laplace and Fourier transforms respectively to the original time dependent data.

We have observed a substantial mismatch of amplitudes between computationally simulated and experimental data. Hence, we have calibrated experimental data here via multiplying them by the calibration factor 10^{-7} , just as in [32, 34, 35].

7.1 Data collection

Our experimental data were collected in the field by the Forward Looking Radar of the US Army Research Laboratory [40]. The schematic diagram of data collection is presented on Figure 4. The device has two sources placed on the top of a car. Sources emit pulses. The device also has 16 detectors. Detectors measure backscattering time resolved signal, which is actually the voltage. Pulses of only one component of the electric field are emitted and the same component is measured on those detectors. The time step size of measurements is 0.133 nanosecond and the maximal amplitudes of the measured signal are seen about 2 nanoseconds, see Figure 5. Since 1 nanosecond corresponds to the frequency of 1 Gigahertz [50], then the corresponding frequency range is in Gigahertz, which are considered as high frequencies in Physics. The car moves and the time dependent backscattering signal is measured on distances from 20 to 8 meters from the target of interest. The collected signals are averaged. Users know horizontal coordinates of each target with a very good precision: to do this, the Ground Positioning System is used. Two kinds of targets were tested: ones located in air and ones buried on the depth of a few centimeters in the ground.

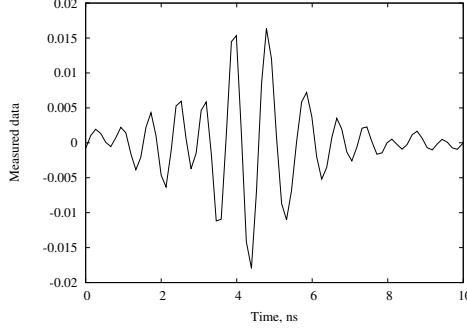


Figure 5: Measured time dependent data for bush after being multiplied by the calibration factor 10^{-7} . The horizontal axis is time in nanoseconds.

7.2 Results

While it is assumed both in (2.1) and (6.5) that $c(x) \geq 1$, we had one target buried in the ground, in which $0 < c < 1$. This target was a plastic cylinder. It was shown on page 2944 of [35] that, using the original time dependent data, one can figure out that inside the target $c \in (0, 1)$. Hence, in this case we replace (6.1) and (6.5) with

$$\tilde{c}_{comp}(x) = 1 - \left| -v''(x, \underline{k}) - \underline{k}^2 (v'(x, \underline{k}))^2 + 2i\underline{k}v'(x, \underline{k}) \right|, \quad (7.1)$$

$$c_{comp}(x) = \begin{cases} \tilde{c}_{comp}(x), & \text{if } \tilde{c}_{comp}(x) \in (0.1, 1), \\ 1, & \text{otherwise.} \end{cases} \quad (7.2)$$

Suppose that a target occupies a subinterval $I \subset (0, 1)$. In fact, we estimate here the ratio of dielectric constants of targets and backgrounds for $x \in I$. Thus, actually our computed function $c_{comp}(x)$ in (6.5) and (7.2) is an estimate of the function $P(x)$,

$$P(x) = \frac{c_{target}(x)}{c_{bckgr}} \approx c_{comp}(x), x \in I, \quad (7.3)$$

where $c_{target}(x)$ is the spatially distributed dielectric constant of that target. Using (6.5), (7.1), (7.2) and (7.3), we define the computed target/background contrast in the dielectric constant as

$$\tilde{P} = \begin{cases} \max c_{comp}(x), & \text{if } c_{comp}(x) \geq 1, \forall x \in [0, 1], \\ \min c_{comp}(x), & \text{if } c_{comp}(x) \leq 1, \forall x \in [0, 1]. \end{cases} \quad (7.4)$$

Finally, we introduce the number c_{est} , which is our estimate of the dielectric constant of a target,

$$c_{est} = c_{bckgr} \tilde{P}. \quad (7.5)$$

We have chosen the interval $[\underline{k}, \bar{k}]$ as

$$k \in [2.7, 3.2] = [\underline{k}, \bar{k}]. \quad (7.6)$$

The considerations for the choice (7.6) were similar with ones for the case of simulated data in section 6.2.

We had experimental data for total five targets. The background was air in the case of targets placed in air with $c_{bckgr} = 1$ and it was sand with $c_{bckgr} \in [3, 5]$ [49] in the case

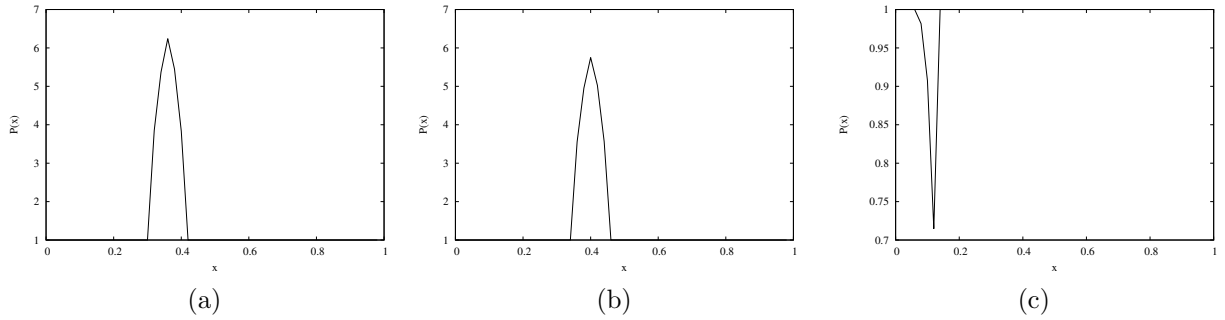


Figure 6: Computed functions $c_{comp}(x)$ for different targets: a) bush in air, b) buried metal cylinder, c) buried plastic cylinder

of buried targets. Two targets, bush and wood stake, were placed in air and three targets, metal box, metal cylinder and plastic cylinder, were buried in sand. Figures 6 display some samples of calculated images of targets.

Dielectric constants of targets were not measured in experiments. So, the maximum what we can do at this point is to compare our computed values of c_{est} with published ones. This is done in Table 1, in which c_{true} is a published value. As to the metallic targets, it was established numerically in [34, 35] that they can be approximated as dielectric targets with large values of the dielectric constant,

$$c \in [10, 30]. \quad (7.7)$$

Published values of dielectric constants of sand, wood and plastic can be found in [49]. As to the case when the target was a bush, we took the interval of published values from [16]. Bush was the most challenging target to image. This is because bush is obviously a significantly heterogeneous target.

| Target | buried/no | \tilde{P} | c_{bckgr} | c_{est} | c_{true} |
|------------------|-----------|-------------|-------------|----------------|------------|
| Bush | no | 6.24 | 1 | 6.24 | [3, 20] |
| Wood stake | no | 5.43 | 1 | 5.43 | [2, 6] |
| Metal box | buried | 5.75 | [3, 5] | [17.25, 28.75] | [10, 30] |
| Metal cylinder | buried | 6.48 | [3, 5] | [19.44, 32.40] | [10, 30] |
| Plastic cylinder | buried | 0.71 | [3, 5] | [2.13, 3.55] | [1.1, 3.2] |

Table 1: Summary of estimated dielectric constants c_{est} .

For the engineering part of this team of coauthors (LN and AS), the depth of burial of a target is not of an interest here since all depths are a few centimeters. It is also clear that it is impossible to figure out the shape of the target, given so limited information content. On the other hand, the most valuable piece of the information for LN and AS is in estimates of the dielectric constants of targets. Therefore, Table 1 is the most interesting piece of the information from the engineering standpoint. Indeed, one can see in this table that values of estimated dielectric constants c_{est} are always within limits of c_{true} . As it was pointed out in section 1, these estimates, even if not perfectly accurate, can be

potentially very useful for the quite important goal of reducing the false alarm rate. This indicates that the technique of the current paper might potentially be quite valuable for the goal of an improvement of the false alarm rate. The above results inspire LN and AS to measure dielectric constants of targets in the future experiments. Our team plans to treat those future experimental data by the numerical method of this publication.

8 Concluding Remarks

We have developed a new globally convergent numerical method for the 1-D Inverse Medium Scattering Problem (2.6). Unlike the tail function method, the one of this paper does not impose the smallness condition on the size of the interval $[\underline{k}, \bar{k}]$ of wave numbers. The method is based on the construction of a weighted cost functional with the Carleman Weight Function in it. The main new theoretical result of this paper is Theorem 4.1, which claims the strict convexity of this functional on any closed ball $\overline{B}(R) \subset H$ for any radius $R > 0$, as long as the parameter $\lambda > 0$ of this functional is chosen appropriately. Global convergence of the gradient method of the minimization of this functional to the exact solution is proved. Numerical testing of this method on both computationally simulated and experimental data shows good results.

References

- [1] A. D. AGALTSOV AND R. G. NOVIKOV, *Riemann-Hilbert problem approach for two-dimensional flow inverse scattering*, Journal of Mathematical Physics, 55 (2014), p. 103502.
- [2] H. AMMARI, Y. T. CHOW, AND J. ZOU, *Phased and Phaseless Domain Reconstructions in the Inverse Scattering Problem via Scattering Coefficients*, SIAM Journal on Applied Mathematics, 76 (2016), pp. 1000–1030.
- [3] H. AMMARI AND H. KANG, *Reconstruction of Small Inhomogeneities from Boundary Measurements*, vol. 1846 of Lecture Notes in Mathematics, Springer Berlin Heidelberg, Berlin, Heidelberg, 2004.
- [4] A. B. BAKUSHINSKII, M. V. KLIBANOV, AND N. A. KOSHEV, *Carleman weight functions for a globally convergent numerical method for ill-posed Cauchy problems for some quasilinear PDEs*, Nonlinear Analysis: Real World Applications, 34 (2017), pp. 201–224.
- [5] G. BAO, P. LI, J. LIN, AND F. TRIKI, *Inverse scattering problems with multi-frequencies*, Inverse Problems, 31 (2015), p. 093001.
- [6] L. BAUDOIN, M. DE BUHAN, AND S. ERVEDOZA, *Global Carleman Estimates for Waves and Applications*, Communications in Partial Differential Equations, 38 (2013), pp. 823–859.
- [7] L. BAUDOIN, M. DE BUHAN, AND S. ERVEDOZA, *Convergent algorithm based on Carleman estimates for the recovery of a potential in the wave equation*, (2016), <https://arxiv.org/abs/1610.07400>.

- [8] L. BEILINA AND M. V. KLIBANOV, *A Globally Convergent Numerical Method for a Coefficient Inverse Problem*, SIAM Journal on Scientific Computing, 31 (2008), pp. 478–509.
- [9] L. BEILINA AND M. V. KLIBANOV, *Approximate global convergence and adaptivity for coefficient inverse problems*, Springer, 2012.
- [10] L. BEILINA AND M. V. KLIBANOV, *Globally strongly convex cost functional for a coefficient inverse problem*, Nonlinear Analysis: Real World Applications, 22 (2015), pp. 272–288.
- [11] A. BUKHGEIM AND M. KLIBANOV, *Uniqueness in the large of a class of multidimensional inverse problems*, Soviet Math. Doklady, 17 (1981), pp. 244—247.
- [12] F. CAKONI AND D. COLTON, *On the mathematical basis of the linear sampling method*, Georgian Mathematical Journal, 10 (2003), pp. 411–426.
- [13] D. CHARALAMBOPOULOS, D. GINTIDES, AND K. KIRIAKI, *The linear sampling method for the transmission problem in three-dimensional linear elasticity*, Inverse Problems, 18 (2002), pp. 547–558.
- [14] G. CHAVENT, *Nonlinear Least Squares for Inverse Problems - Theoretical Foundations and Step-by-Step Guide for Applications*, Springer, 2009.
- [15] Y. T. CHOW AND J. ZOU, *A Numerical Method for Reconstructing the Coefficient in a Wave Equation*, Numerical Methods for PDEs, 31 (2015), pp. 289–307.
- [16] H. T. CHUAH, K. Y. LEE, AND T. W. LAU, *Dielectric Constants of Rubber and Oil Palm Leaf Samples at X-Band*, IEEE Transactions on Geoscience and Remote Sensing, 33 (1995), pp. 221–223.
- [17] H. W. ENGL, M. HANKE AND A. NEUBAUER, *Regularization of inverse problems*, Kluwer Academic Publishers, Boston, 2000.
- [18] A. GONCHARSKY AND S. ROMANOV, *Supercomputer technologies in inverse problems of ultrasound tomography*, Inverse Problems, 29 (2013), p. 075004.
- [19] A. V. GONCHARSKY AND S. Y. ROMANOV, *Iterative methods for solving coefficient inverse problems of wave tomography in models with attenuation*, Inverse Problems, 33 (2017), p. 025003.
- [20] K. ITO, B. JIN, AND J. ZOU, *A direct sampling method for inverse electromagnetic medium scattering*, Inverse Problems, 29 (2013), p. 095018.
- [21] S. KABANIKHIN, K. SABELFELD, N. NOVIKOV, AND M. SHISHLENIN, *Numerical solution of the multidimensional Gelfand-Levitan equation*, J. Inverse and Ill-Posed Problems, 23 (2015), pp. 439–450.
- [22] A. KIRSCH AND N. GRINBERG, *The factorization method for inverse problems*, Oxford Lecture Series in Mathematics and its Applications, Oxford University Press, Oxford, 2008.

- [23] A. L. KARCHEVSKY, M.V. KLIBANOV, L.NGUYEN, N. PANTONG AND A. SULLIVAN, *The Krein Method and the Globally Convergent Method for Experimental Data*, *Applied Numerical Mathematics*, 74 (2013), pp. 111-127.
- [24] M. V. KLIBANOV AND O. V. IOUSSOUPOVA, *Uniform Strict Convexity of a Cost Functional for Three-Dimensional Inverse Scattering Problem*, *SIAM Journal on Mathematical Analysis*, 26 (1995), pp. 147–179.
- [25] M. V. KLIBANOV, *Global Convexity in a Three-Dimensional Inverse Acoustic Problem*, *SIAM Journal on Mathematical Analysis*, 28 (1997), pp. 1371–1388.
- [26] M. V. KLIBANOV AND A. TIMONOV, *Carleman Estimates for Coefficient Inverse Problems and Numerical Applications*, de Gruyter, Utrecht, 2004.
- [27] M. V. KLIBANOV, *Carleman estimates for global uniqueness, stability and numerical methods for coefficient inverse problems*, *Journal of Inverse and Ill-Posed Problems*, 21 (2013), pp. 477–560.
- [28] M. V. KLIBANOV, *Carleman weight functions for solving ill-posed Cauchy problems for quasilinear PDEs*, *Inverse Problems*, 31 (2015), p. 125007.
- [29] M. V. KLIBANOV AND V. G. KAMBURG, *Globally strictly convex cost functional for an inverse parabolic problem*, *Mathematical Methods in the Applied Sciences*, 39 (2016), pp. 930–940.
- [30] M. V. KLIBANOV, N. A. KOSHEV, J. LI, AND A. G. YAGOLA, *Numerical solution of an ill-posed Cauchy problem for a quasilinear parabolic equation using a Carleman weight function*, *Journal of Inverse and Ill-posed Problems*, 24 (2016), pp. 761–776.
- [31] M. V. KLIBANOV, D.-L. NGUYEN, L. H. NGUYEN, AND H. LIU, *A globally convergent numerical method for a 3D coefficient inverse problem with a single measurement of multi-frequency data*, (2016), <https://arxiv.org/abs/1612.04014>.
- [32] M. V. KLIBANOV, L. H. NGUYEN, A. SULLIVAN, AND L. NGUYEN, *A globally convergent numerical method for a 1-d inverse medium problem with experimental data*, *Inverse Problems and Imaging*, 10 (2016), pp. 1057–1085.
- [33] M. V. KLIBANOV AND N. T. THÀNH, *Recovering Dielectric Constants of Explosives via a Globally Strictly Convex Cost Functional*, *SIAM Journal on Applied Mathematics*, 75 (2015), pp. 518–537.
- [34] A. V. KUZHUGET, L. BEILINA, M. V. KLIBANOV, A. SULLIVAN, L. NGUYEN, AND M. A. FIDDY, *Blind backscattering experimental data collected in the field and an approximately globally convergent inverse algorithm*, *Inverse Problems*, 28 (2012), p. 095007.
- [35] A. V. KUZHUGET, L. BEILINA, M. V. KLIBANOV, A. SULLIVAN, L. NGUYEN, AND M. A. FIDDY, *Quantitative Image Recovery From Measured Blind Backscattered Data Using a Globally Convergent Inverse Method*, *IEEE Transactions on Geoscience and Remote Sensing*, 51 (2013), pp. 2937–2948.

- [36] J. LI, H. LIU, AND J. ZOU, *Locating Multiple Multiscale Acoustic Scatterers*, Multiscale Modeling & Simulation, 12 (2014), pp. 927–952.
- [37] J. J. LIU AND M. SINI, *On the Accuracy of the Numerical Detection of Complex Obstacles from Far Field Data Using the Probe Method*, SIAM Journal on Scientific Computing, 31 (2009), pp. 2665–2687.
- [38] D.-L. NGUYEN, *The factorization method for the Drude-Born-Fedorov model for periodic chiral structures*, Inverse Problems and Imaging, 10 (2016), pp. 519–547.
- [39] D.-L. NGUYEN, M. V. KLIBANOV, L. H. NGUYEN, A. E. KOLESOV, M. A. FIDDY, AND H. LIU, *Numerical Solution of a Coefficient Inverse Problem with Multi-Frequency Experimental Raw Data by a Globally Convergent Algorithm*, (2016), <https://arxiv.org/abs/1609.03102>.
- [40] L. NGUYEN, D. WONG, M. RESSLER, F. KOENIG, B. STANTON, G. SMITH, J. SICHINA, AND K. KAPPRA, *Obstacle avoidance and concealed target detection using the Army Research Lab ultra-wideband synchronous impulse reconstruction (UWB SIRE) forward imaging radar*, 2007, p. 65530H.
- [41] R. NOVIKOV, *The inverse scattering problem on a fixed energy level for the two-dimensional Schrödinger operator*, Journal of Functional Analysis, 103 (1992), pp. 409–463.
- [42] R. G. NOVIKOV, *Multidimensional inverse spectral problem for the equation $-\delta\psi + (v(x) - Eu(x))\psi = 0$* , Functional Analysis and Its Applications, 22 (1989), pp. 263–272.
- [43] R. G. NOVIKOV, *An iterative approach to non-overdetermined inverse scattering at fixed energy*, Sbornik: Mathematics, 206 (2015), pp. 120–134.
- [44] J. A. SCALES, M. L. SMITH, AND T. L. FISCHER, *Global optimization methods for multimodal inverse problems*, Journal of Computational Physics, 103 (1992), pp. 258–268.
- [45] M. SINI AND N. T. THÀNH, *Inverse acoustic obstacle scattering problems using multifrequency measurements*, Inverse Problems and Imaging, 6 (2012), pp. 749–773.
- [46] M. SINI AND N. T. THÀNH, *Regularized recursive Newton-type methods for inverse scattering problems using multifrequency measurements*, ESAIM: Mathematical Modelling and Numerical Analysis, 49 (2015), pp. 459–480.
- [47] M. SOUMEKH, *Synthetic aperture radar signal processing with MATLAB algorithms*, John Wiley & Sons, New York, 1999.
- [48] N. T. THÀNH, L. BEILINA, M. V. KLIBANOV, AND M. A. FIDDY, *Imaging of Buried Objects from Experimental Backscattering Time-Dependent Measurements Using a Globally Convergent Inverse Algorithm*, SIAM Journal on Imaging Sciences, 8 (2015), pp. 757–786.
- [49] *Dielectric Constant Table*, <https://www.honeywellprocess.com/library/marketing/tech-s>

[50] *Unit Converter*, [https://www.unitjuggler.com/convert-frequency-from-GHz-to-ns\(p\).h](https://www.unitjuggler.com/convert-frequency-from-GHz-to-ns(p).h)